Thermal resistance of twist boundaries in silicon nanowires by nonequilibrium molecular dynamics

Cite as: AIP Advances **7**, 045105 (2017); https://doi.org/10.1063/1.4979982
Submitted: 13 January 2017 . Accepted: 29 March 2017 . Published Online: 05 April 2017

Jan K. Bohrer, Kevin Schröer, Lothar Brendel, and Dietrich E. Wolf

AIP ADVANCES 7, 045105 (2017)

Thermal resistance of twist boundaries in silicon nanowires by nonequilibrium molecular dynamics

Jan K. Bohrer, Kevin Schröer,[a] Lothar Brendel, and Dietrich E. Wolf
Department of Physics and Center for Nanointegration Duisburg-Essen (CENIDE), Universität Duisburg-Essen, D-47048 Duisburg, Germany

(Received 13 January 2017; accepted 29 March 2017; published online 5 April 2017)

The thermal boundary resistance (Kapitza resistance) of (001) twist boundaries in silicon is investigated by nonequilibrium molecular dynamics simulations. In order to enable continuous adjustment of the mismatch angle, a cylindrical geometry with fixed atomic positions at the boundaries is devised. The influence of the boundary conditions on the Kapitza resistance is removed by means of a finite size analysis. Due to the diamond structure of silicon, twist boundaries with mismatch angles ϕ and $90° - \phi$ are not equivalent, whereas those with $\pm\phi$ or with $90° \pm \phi$ are. The Kapitza resistance increases with mismatch angle up to 45°, where it reaches a plateau around 1.56 ± 0.05 K m^2/GW. Between 80° and the 90° $\Sigma 1$ grain boundary it drops by about 30%. Surprisingly, lattice coincidence at other angles ($\Sigma 5$, $\Sigma 13$, $\Sigma 27$, $\Sigma 25$) has no noticable effect on the Kapitza resistance. However, there is a clear correlation between the Kapitza resistance and the width of a non-crystalline layer at the twist boundaries. [http://dx.doi.org/10.1063/1.4979982]

I. INTRODUCTION

Due to its high Seebeck coefficient α and (dopant dependent) electrical conductivity σ, silicon would be a promising thermoelectric material with a decent figure of merit zT,

$$zT = \frac{\alpha^2 \sigma}{\kappa} T\,, \tag{1}$$

if its thermal conductivity κ were lower than it is in a single crystal. It has been shown[1] that this can be achieved in nano-crystalline silicon (grain sizes in the order of 25 nm), where phononic heat conduction is suppressed by grain boundaries.[2] This raises the question, what type of grain boundaries are most efficient in doing so. Nonequilibrium molecular dynamics (NEMD) can give an answer, provided a number of technical problems related to the geometric simulation setup can be solved. This paper shows how this can be done.

Grain boundaries are characterised by 5 degrees of freedom: Three fix the relative crystallographic orientation of the adjacent grains, and two fix the normal direction of the grain boundary. An exhaustive scan of the 5-dimensional parameter space, however, is not intended here. We restrict ourselves to twist boundaries with normal direction in (001). The grains are rotated relative to each other around the (001) axis by an angle ϕ, called the mismatch (or twist) angle.

We investigate the dependence of the thermal resistance of twist boundaries on the mismatch angle. Based on results of former MD simulations for silicon and diamond grain boundaries,[3–5] we expect interfacial resistances in the order of a few K m^2/GW and an increase with the twist angle up to at least 40°. So far only a few special mismatch angles, characterized by a certain degree of lattice coincidence in both grains, were studied. Our aim is to simulate the thermal processes between

[a]Electronic mail: kevin.schroeer@uni-due.de

two grains with arbitrary mismatch angle. This cannot be done with periodic boundary conditions in the plane parallel to the twist boundary. Instead we simulate a cylindrical sample with fixed atomic positions at its boundary. This method is described in section II. A systematic finite size analysis allows to get rid of the influence of the boundary. This is one of the results presented in section III. Conclusions from the results are drawn in the final section IV.

II. METHODS

Thermal transport in silicon is simulated by nonequilibrium molecular dynamics (NEMD) using the Stillinger-Weber potential with original parameters,[6] which is well characterized and was shown to produce realistic results in previous studies.[3,5,7,8] For our simulations, we used the well established program LAMMPS.[9]

To obtain rotational symmetry, we choose a cylindrical geometry for the investigated nanowires, as shown in Fig. 1. A shell of fixed atomistic walls is used, which has a thickness of 1.2 lattice constants along the wire and one lattice constant at both ends. Both the mobile part and the fixed walls consist of isotopically pure ^{28}Si. Particle-wall interactions are described by the same potential as particle-particle interactions. This fixed shell allows for arbitrary twist angles at the grain boundary as explained in Sec. II B.

The following method is used to establish a constant one dimensional heat flux j through the system (defining the z direction): A slab of the nanowire (thickness L_H) at one end is heated by adding a certain amount of kinetic energy ΔK per time step Δt to the atoms by rescaling their velocity vectors accordingly. The slab at the other end (thickness $L_\mathrm{C} = L_\mathrm{H}$) is cooled by the same method, extracting the same amount of kinetic energy per time step and thus maintaining energy conservation of the whole system. The heating and cooling regions are scaled with the system length L having always a thickness of $L/22$. This scheme was preferred over the Müller-Plathe method,[10] because that also incorporates fluctuations in the heat flux instead of being a constant external control parameter.

In the stationary state, the heat flux density is homogeneous and amounts to

$$j = \frac{\Delta K}{\Delta t\, A}\,, \tag{2}$$

where A is the cross sectional area of the cylindrical nanowire. The local instantaneous temperature T is defined by dividing the wire into slabs (with thickness of one lattice constant a_0) and accordingly averaging the kinetic energy K_int of the contained inner degrees of freedom N_int at a given time step,

$$T := \frac{2\,K_\mathrm{int}}{N_\mathrm{int}\,k_\mathrm{B}}\,, \tag{3}$$

where k_B is the Boltzmann constant. This instantaneous temperature is then averaged over a time interval to produce a temperature profile $T(z)$, which, in the stationary state, does not depend on time except for statistical fluctuations.

Initially, the atoms are placed at the 0 K equilibrium positions of the silicon lattice and are given random velocities corresponding to a Maxwell-Boltzmann distribution with a temperature of

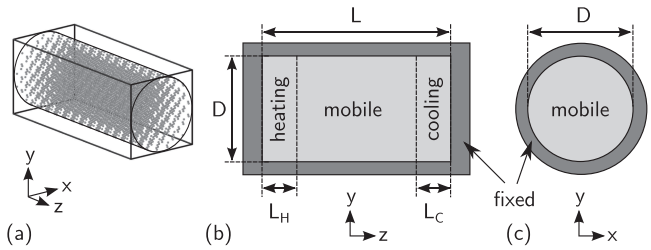

FIG. 1. Simulated system with fixed atomistic boundary conditions: (a) The simulated mono-crystalline nanowire of cylindrical shape contains ^{28}Si isotopes, which are initially placed at their equilibrium positions at $T = 0$ K. (b, c) The Si-wire is completely enclosed in a cylindrical shell of fixed Si-atoms. The dimensions of the mobile part are diameter D and length L, which includes the heating and cooling layers (lengths $L_\mathrm{H,C}$), where kinetic energy is injected and withdrawn, respectively. The z-axis is parallel to the [001]-direction of the crystal lattice.

300 K. Thereafter, the MD simulation with a time step of 1 fs consists of two phases: First, the system is equilibrated for 3 ns at 300 K using the Nosé-Hoover-thermostat[11] with constant volume V and constant number of particles N (NVT-ensemble). For large systems ($L > 170\ a_0$ or $A \geq 200\ a_0^2$) this equilibration time is extended to 4 ns. Second, the thermostat is switched off and the heat flux is established and maintained for 6 ns in the NVE-ensemble. In this second phase, the system is given a time of 3 ns to reach the stationary state and the last 3 ns are used to measure and average the temperature profiles. The heat flux density is chosen to be the same for all investigated systems ($j = 21.73\ \mathrm{GW/m^2}$).

A. Measuring thermal conductivity

At first, we investigate the thermal properties of crystalline nanowires devoid of any grain boundary (GB). Knowing the heat flux and the temperature profile $T(z)$ from the simulation, the thermal conductivity κ is determined from Fourier's law (in one dimension):

$$j = -\kappa \frac{dT}{dz}\,. \tag{4}$$

If Fourier's law is valid and j is constant, we expect a linear temperature profile, provided κ does not vary too much spatially. Figure 2 shows that linearity is given in the middle of the nanowire. At the ends, where the heating and cooling takes place, Fourier's law does not apply. That is because in the heat source and sink, the system is externally perturbed by rescaling the velocities and can not reach local equilibrium, which also influences the adjacent regions. The nonlinear behavior was reported by other authors,[8,12] and accounted for by the modified phonon scattering at the heating and cooling regions.

Therefore, the profiles are fitted in the linear range and κ is calculated from Eq. (4). To prove consistency, we simulate the same system several times, only changing the seed of the random number generator that creates the initial velocity distribution. Although the different profiles in Fig. 2 do not vary much in the graphical representation, numerical evaluation shows that the value for κ varies about 1%.

To account for these statistical variations, we average the temperature profiles of the different seeds: After choosing a region of appropriate size ℓ for the linear fit (shown in Fig. 2 and Fig. 5), its average temperature was subtracted for each sample to get rid of small total energy differences left from the thermalization phase. Afterwards, the slope was calculated from the union of all samples and its error was estimated as $2\sigma/\ell$, where σ^2 is the average of the local variance of the temperature values.

B. Grain boundaries and Kapitza resistance

To implement a twist grain boundary of a certain angle ϑ, one half of the cylindrical monocrystalline nanowire is rotated with respect to the other by ϑ, including the fixed walls, as can be seen

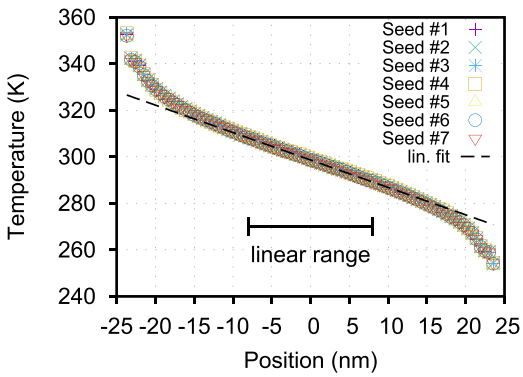

FIG. 2. Steady state temperature profiles averaged over 3 ns for a constant heat flux through a system of $L = 47.8$ nm and $D = 6.13$ nm without grain boundary. For the same geometrical system, different initial velocity distributions constituting the same initial temperature were generated. Seven such simulations show minor variations in the temperature profiles. The thermal conductivity is calculated from the slope of the averaged profile in the linear range.

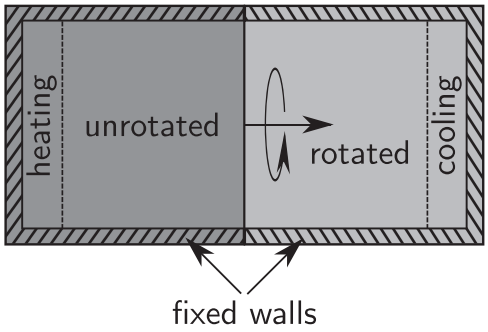

FIG. 3. One half of the cylinder, i.e., all atoms with positions $z > 0$, are rotated by an angle ϑ around an [001]-axis situated in the center of the cylinder cross section. The (001)-rotation plane lies in the x-y-plane and defines the position of the grain boundary. The rotation includes the affected atoms of the fixed walls.

in Fig. 3. The rotation plane (x-y) is an (001)-plane of the diamond lattice. This prescribes the initial atom configuration. We simulate GB systems with and without a coincidence site lattice (CSL).[13] The former are called Σ grain boundaries. Σ corresponds to the size of the primitive unit cell of the CSL relative to the original primitive unit cell of silicon.

We choose fixed boundary conditions, because we want to be able to investigate arbitrary grain boundary twist angles. For periodic boundary conditions, only some specific angles, which create a coincidence site lattice, would be possible to simulate.[3] Furthermore, rotation symmetry is necessary for fixed boundary conditions to obtain equivalent regions on both sides of the grain boundary planes. This, in the end, is the reason for using systems with cylindrical geometry.

During the thermostat phase, an amorphous region emerges at the grain boundary. A common neighbor analysis (CNA[14]), performed within a region of 20 (004) crystal planes centered at the grain boundary and with a cutoff radius of 0.921 a_0, shows which atoms are considered to be in a crystalline environment of the diamond lattice and which have no crystalline order, i.e. are of amorphous structure type (see Fig. 4).

The thickness of the amorphous region turns out to be between one and three lattice constants, depending on the twist angle and the system dimensions and is estimated as follows. For comparison of different grain boundaries, we define a measure for the thickness of the amorphous layer L_{am},

$$L_{\mathrm{am}} = \frac{L_{\mathrm{plane}}}{N_{\mathrm{plane}}} N_{\mathrm{am}} \,, \tag{5}$$

where $L_{\mathrm{plane}} = a_0/4$ is the (004) interplanar distance, N_{plane} is the average number of mobile atoms in these planes and N_{am} is the total number of atoms with amorphous structure type in the considered region of 20 crystal planes. The standard deviation is estimated via the joint variances of averaging over different seeds and points in time.

The grain boundaries constitute a resistance to thermal transport, called Kapitza resistance R_{K}. In the presence of a heat flux, it leads to a temperature discontinuity ΔT at the interface,

$$\Delta T = R_{\mathrm{K}}\, j \,, \tag{6}$$

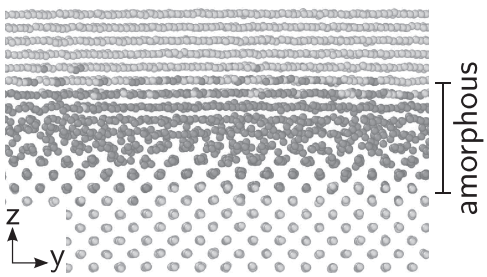

FIG. 4. After thermostating the 36.87° Σ5 grain boundary system to 300 K, the atomic structure is examined by using common neighbor analysis. The atoms in light gray reside in a diamond lattice structure, while the dark gray atoms have no crystalline order and constitute the amorphous region.

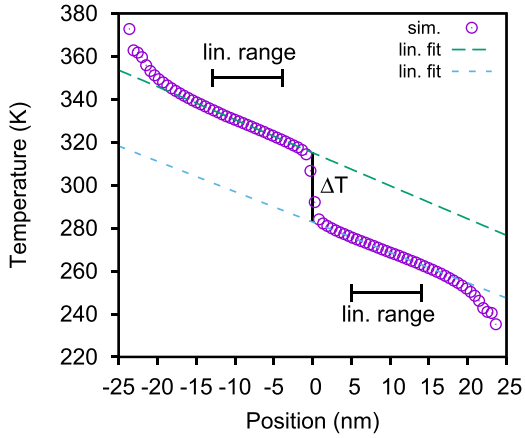

FIG. 5. Measured temperature profile (sim.) averaged over 3 ns for a 36.87° Σ5 grain boundary system of $L = 47.8$ nm and $D = 6.13$ nm. The temperature gap ΔT is determined by extrapolating the two linear ranges and taking the difference of the linear fits at the grain boundary interface.

which is visible in the simulated profiles (see Fig. 5).

The temperature jump is determined by extrapolating the linear ranges on both sides of the grain boundary and taking the difference of the linear fits at the interface (see Fig. 5). Knowing the constant heat flux, the Kapitza resistance is then calculated using Eq. (6).

Again, the consistency of the results is checked by comparing simulation runs with different initial velocity distributions which exhibit similar deviations between each other like in the GB-free case (see Fig. 2). Therefore the profiles are averaged, in the same manner as for the GB-free systems (cf. Sec. II A), to create a mean profile with statistical error bars for each data point. The Kapitza resistance and its uncertainty are determined from the linear fits to this mean profile.

III. RESULTS AND DISCUSSION

In this section, we analyze finite size effects on the thermal properties of systems with and without grain boundary to discuss the influence of the chosen geometry and fixed boundary conditions. We then present our results of the Kapitza resistance measurements for GB systems with 33 different twist angles.

A. Finite size effects on the thermal conductivity

The mono-crystalline, cylindrical system is simulated for four different wire lengths from 23.9 nm to 191 nm with a constant diameter of 6.13 nm. Figure 6 shows an increase of the thermal conductivity with length and lies between 11.6 W m^{-1} K^{-1} and 40.9 W m^{-1} K^{-1}. Schelling *et al.* reported a similar

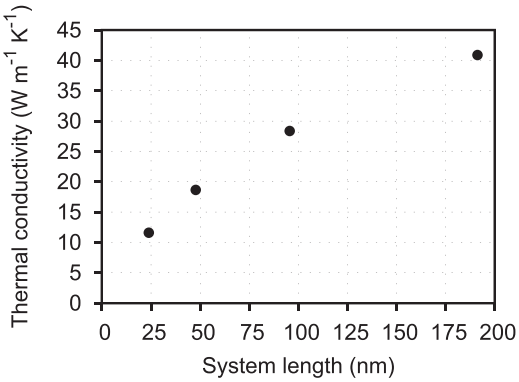

FIG. 6. Variation of thermal conductivity with system length for a system without grain boundary of constant diameter of $D = 6.13$ nm at $T = 300$ K. Error bars are smaller than 1.8 % and not visible in this representation.

behavior (increase of κ with system length) for periodic boundary conditions due to the reduction of the phonon mean free path.

Likewise, we vary the diameter six times between 2.45 nm and 12.26 nm for a constant length of 47.8 nm to investigate the influence of the cross section. As can be seen in Fig. 7, the thermal conductivity also increases with diameter and attains values between 15.5 W m^{-1} K^{-1} and 22.2 W m^{-1} K^{-1}. However, the system length's influence on the heat conduction is much stronger than the diameter's.

It is well known from experiment and simulation that heat conduction is reduced in nano-sized and nano-crystalline media.[8,12,15] By comparing our results to experimental values of $\kappa \approx 250$ W m^{-1} K^{-1} for bulk ^{28}Si,[16] we can confirm a reduction of the thermal conductivity in nanowires by one to two orders of magnitude.

Da Cruz *et al.*[8] used NEMD to study the thermal transport in nanowires of square cross section for different potentials and boundary conditions. They reported similar finite size effects, i.e., increase of the thermal conductivity with length and cross sectional area A. For fixed atomistic boundary conditions and and the Stillinger-Weber potential, they measured $\kappa \approx 15.5$ W m^{-1} K^{-1} for a length of 27.2 nm and cross section of 4.34 nm × 4.34 nm = 18.8 nm^2.

For a further investigation and comparison, we simulate a nanowire with square cross section of $A = 29.5$ nm^2 and $L = 23.9$ nm, leading to $\kappa = 15.2$ W m^{-1} K^{-1}. Extrapolating to the dimensions used by da Cruz *et al.* (stated above), we obtain $\kappa = 15.9$ W m^{-1} K^{-1}, which is in good agreement with their result of 15.5 W m^{-1} K^{-1}.

Comparing the cuboidal setup with our cylindrical system of same length and cross sectional area, i.e. $L = 23.9$ nm and $D = 6.13$ nm, we note a reduction in the thermal conductivity to 11.6 W m^{-1} K^{-1}. Thus, by solely changing the shape of the cross section from square to circular, the heat conduction is reduced by ~ 25%. We attribute this to inadequacies of the MD simulation, especially in combination with fixed boundary conditions:

For the square cross section, the mobile part of the system consists of entire cubic unit cells. For the cylindrical geometry the unit cells near the walls will be cut into regions of mobile and fixed atoms. We propose that the reduction in thermal conductivity is a consequence of the less regular and less periodic particle-wall bonds, which introduce additional phonon scattering. Additionally, da Cruz *et al.*[8] observed that, for simulated nanowires, the thermal conductivity is about twice as high for fixed boundary conditions as for free boundary conditions in the transversal (x-y) directions.

Due to the challenge of characterizing nano scale systems experimentally and the imperfect material properties, comparison with real systems is difficult. Li *et al.*[15] investigated isotopically natural, intrinsic, crystalline Si nanowires with diameters of 22 nm and a length of several microns, measuring thermal conductivities of about 7 W m^{-1} K^{-1} at 300 K. Moreover, the results of Boukai *et al.*[17] indicated experimental values of about 0.8 W m^{-1} K^{-1} for highly doped Si nanowires with cross sectional areas of 10 nm × 20 nm, and of roughly 3.5 W m^{-1} K^{-1} for $A = 20$ nm × 20 nm. Here, the wires were also several microns long.

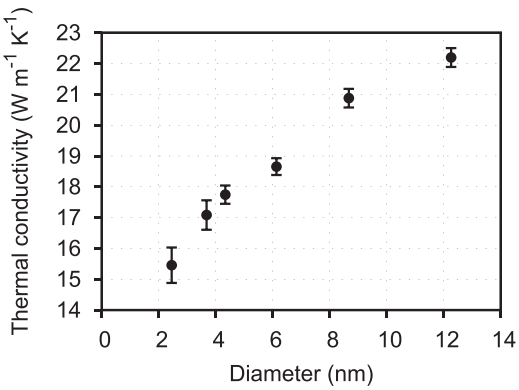

FIG. 7. Variation of thermal conductivity with diameter for a system without grain boundary of length $L = 47.8$ nm at $T = 300$ K.

We compare those values to $\kappa = 22.2\ \mathrm{W\,m^{-1}\,K^{-1}}$ for our largest simulated diameter of 12.3 nm (and $L = 47.8$ nm). Based on the preceding considerations, we conclude an overestimation of the heat conduction in our simulated systems compared to natural and doped Si nanowires. Reasons are the artificial fixed boundary conditions, the isotopic purity, the perfection of the crystal lattice and material surface without impurities or oxidation, and, most importantly for small systems, the disregard of quantum mechanical effects, which will lead to significant variations, even for a temperature of 300 K.[7]

Nevertheless, NEMD can give important information for thermal processes under perfect conditions and indications of the thermal properties. Moreover, it is most useful to investigate the influence of parameter variations by tendency, like scaling dimensions, or, in our case, varying the grain boundary twist angle (see Sec. III C).

B. Finite size effects on the Kapitza resistance

Next, we present our results for the grain boundary systems, investigating the influence of length, diameter, and, in Sec. III C, twist angle variations on the thermal boundary resistance. The 36.87° Σ5 GB system with $D = 6.13$ nm is simulated for five different lengths from 23.9 nm to 382 nm, leading to a Kapitza resistance in the range from 1.46 K m^2/GW to 1.53 K m^2/GW (see Fig. 8). Although the shortest and longest system have the highest and lowest resistance, respectively, we can not conclude a systematic trend in the light of the given uncertainties. In fact, except for the highest value, the deviation from the mean is covered by the error bars and the highest deviation amounts to 2.4% (see Fig. 8). While we can not exclude a possible influence of the system length on the Kapitza resistance, the results state that it is of minor importance for the considered dimensions. Schelling *et al.*[3] used NEMD with periodic boundary conditions to study heat conduction in Si Σ grain boundaries. They also report very little effect of length variations on the Kapitza resistance for the 43.6° (001) GB system.

A variation of the diameter, on the other hand, leads to a strong and systematic behavior of the Kapitza resistance. We examine systems with a constant length of 47.8 nm and varying diameters from 4.33 nm to 12.3 nm for four different twist angles. As can be seen in Fig. 9, the Kapitza resistance shows a decreasing and converging trend with increasing cross sectional area. Plotting the inverse of R_K versus inverse area leads to data that is in good agreement with a linear fit. We therefore formulate the approach

$$\frac{1}{R_\mathrm{K}(\vartheta)} = \frac{1}{R_\mathrm{inf}(\vartheta)} - \frac{\gamma(\vartheta)}{A}\,, \tag{7}$$

with $A = \pi D^2/4$ and individual fit parameters R_inf and γ for each ϑ (cf. Table I). Multiplying with A, this equation can be interpreted as the conductance for infinite cross section $G_\mathrm{inf} = A/R_\mathrm{inf}$ being reduced by a constant γ. While the detailed mechanism behind this "lost conductance channel" remains unclear, one can calculate the area A_0 for which the conductance would vanish. It amounts to about 4.5 nm^2 (corresponding to 15 unit cells) and suggests an area independent boundary effect due to the fixed atomic shell of the cylinder geometry.

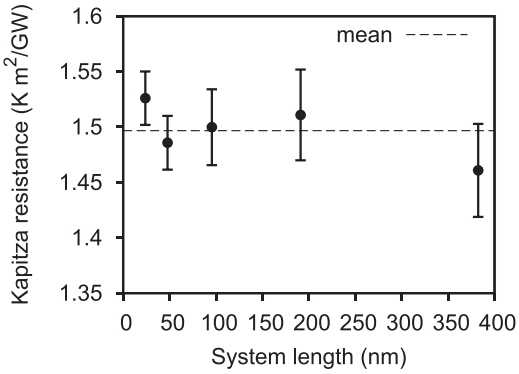

FIG. 8. Variation of the Kapitza resistance with system length for a 36.87° Σ5 grain boundary system with a constant diameter of $D = 6.13$ nm at $T = 300$ K.

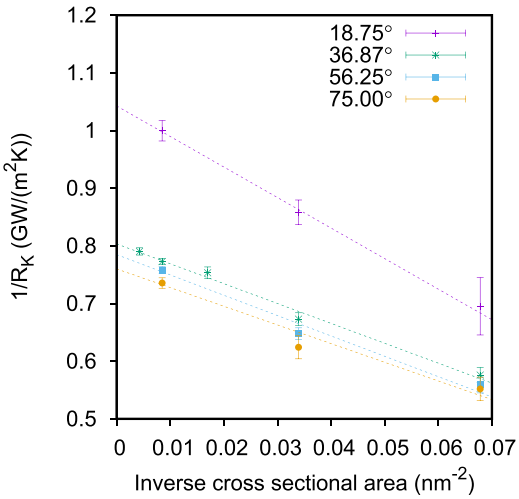

FIG. 9. Variation of the inverse Kapitza resistance R_K^{-1} with cross sectional area for grain boundary systems with a constant length of $L = 47.8$ nm and four different twist angles (given in the legend) at $T = 300$ K. The inverse Kapitza resistance shows linear behavior with inverse area. The value for infinite cross section is estimated by extrapolation.

We eliminate the influence of the fixed boundary conditions by extrapolating to infinite cross sectional area, as for $A \to \infty$, all types of lateral boundary conditions (free, fixed, and periodic in x-y-directions) and different geometries should converge to the same results.

The data show deviations of the Kapitza resistances from R_{inf} of $\leq 5\%$ for diameters $D > 12.3$ nm and $\leq 18\%$ for diameters $D > 6.1$ nm (see Table I and Fig. 9). Due to the high computational effort for big systems, we use $D = 6.13$ nm and $L = 47.8$ nm to investigate the twist angle's influence in Sec. III C. If necessary, we are then able to extrapolate to infinite cross section by reducing the boundary resistance by about 18%. While this finite size analysis was done for the four presented twist angles, we expect similar behavior for other angles, and use the same scaling law.

C. Dependence of the Kapitza resistance on the grain boundary angle

We investigate 25 twist angles from 3.75° to 93.75° in equal steps of 3.75°. Due to the twofold symmetry of the diamond lattice, angles of $90° \pm \phi$ have equivalent configurations and should lead to the same results. This is verified for our simulations by comparing the 86.25° and 93.75° angle systems, which indeed yield the same Kapitza resistance of 1.48 K m^2/GW (see Fig. 10).

Additionally, we simulate eight GB systems with coincidence site lattices. Here, the five smallest Σ values are chosen for investigation. Thus, including the 90° Σ1 GB, we study nine Σ grain boundaries (see Table II) and a total of 33 GB systems. The determined values of the thermal boundary resistance for all angles are summarized in Table III.

Within the error bars, Fig. 10 shows a monotonous increase of the Kapitza resistance with twist angle up to 41.25°. For larger angles, i.e., from 41.25° to 82.5°, R_K is nearly constant with fluctuations about a mean of approximately 1.55 K m^2/GW, as can also be seen in more detail in the given inset. We note a drop in R_K of about 30% for the special Σ1 GB at 90°. Besides this case,

TABLE I. Kapitza Resistance for four different twist angles extrapolated to infinite cross section R_{inf} compared to a reference systems of $D = 6.13$ nm and $L = 47.8$ nm (R_{ref}). The linear fit parameter γ (in nm^2 (m^2 K/GW)$^{-1}$) is given according to Eq. (7) for each angle. All uncertainties are twice the standard deviation.

ϑ (°)	R_{inf} (K m^2/GW)	$(R_{ref} - R_{inf})/R_{ref}$	γ
18.75	0.96 ± 0.01	0.18 ± 0.03	5.29 ± 0.53
36.87	1.24 ± 0.01	0.16 ± 0.02	3.45 ± 0.38
56.25	1.27 ± 0.05	0.17 ± 0.04	3.53 ± 0.96
75.00	1.32 ± 0.05	0.18 ± 0.06	3.24 ± 1.05

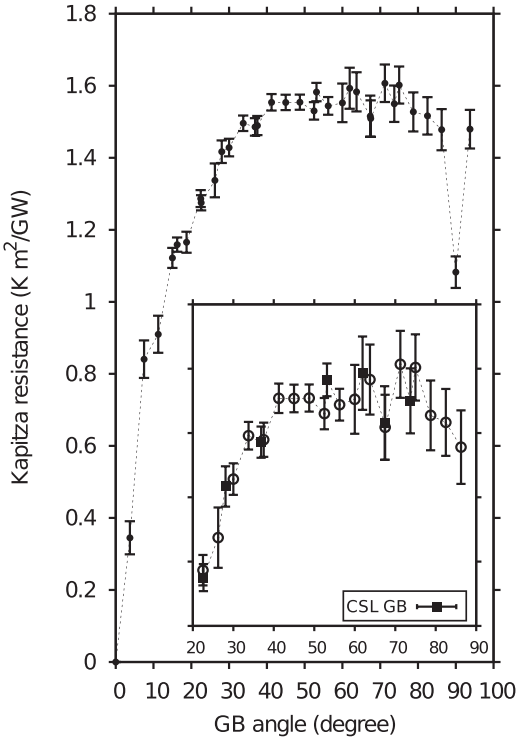

FIG. 10. Dependence of the Kapitza resistance on the grain boundary twist angle for a system length of $L = 47.8$ nm and diameter of $D = 6.13$ nm at $T = 300$ K. The inset shows a detailed excerpt for angles from 22.5° to 86.25°. The eight Σ grain boundaries (CSL GB) are marked.

based on our results, we cannot state that Σ grain boundaries have distinguished heat conduction properties compared to grain boundaries with similar angles. While e.g. the 51.13° Σ5 GB seems to constitute a local maximum, this can easily be caused by statistical uncertainties, considering the magnitude of the error bars (see the inset in Fig. 10). The same applies to the local minima at some of the other Σ angles (36.87°, 67.38°, and 73.74°). Although it seems plausible to assume a modified heat conduction in CSLs due to the increased periodicity of the superlattice, we cannot confirm this behavior.

The thickness L_{am} of the amorphous layer, measured as described in Sec. II B and displayed in Fig. 11, can shed some light on this result: It increases steeply and monotonously with the twist angle up to 15° and stays essentially constant for larger angles, except for a distinctive drop at the Σ1 GB at 90°. While it saturates earlier than the Kapitza resistance (shown in Fig. 11, as well), the correlation between them is evident. That is, R_{K} is much more dominated by the existence and thickness of the amorphous layer than by a possible superlattice. Actually, the former can be the reason for the irrelevance of the latter: Only in the absence of such a disordered layer, the mismatch strain in the boundary region would decrease with increasing number of coincident sites.

TABLE II. The nine investigated Σ grain boundaries. There are two twist angles ($\vartheta_{1,2}$) for every Σ value, symmetric about 45°. As a trivial case, the 0° mono-crystalline system has no grain boundary and is listed in parenthesis for reasons of clarity.

Σ	ϑ_1 (°)	ϑ_2 (°)
25	16.26	73.74
13	22.62	67.38
17	28.07	61.93
5	36.87	53.13
1	(0.00)	90.00

TABLE III. Determined values of the Kapitza resistance for the 33 investigated (001) GB systems with twist angles ϑ at $T = 300$ K. Dimensions of the simulated nanowires are $L = 47.8$ nm and $D = 6.13$ nm.

ϑ (°)	R_K (K m^2/GW)	ϑ (°)	R_K (K m^2/GW)
3.75	0.34 ± 0.05	48.75	1.55 ± 0.02
7.50	0.84 ± 0.05	52.50	1.53 ± 0.02
11.25	0.91 ± 0.05	53.13	1.58 ± 0.03
15.00	1.12 ± 0.03	56.25	1.54 ± 0.02
16.26	1.16 ± 0.02	60.00	1.55 ± 0.05
18.75	1.17 ± 0.03	61.93	1.59 ± 0.06
22.50	1.29 ± 0.02	63.75	1.58 ± 0.05
22.62	1.28 ± 0.02	67.38	1.52 ± 0.06
26.25	1.34 ± 0.05	67.50	1.51 ± 0.05
28.07	1.42 ± 0.03	71.25	1.61 ± 0.05
30.00	1.43 ± 0.02	73.74	1.55 ± 0.05
33.75	1.50 ± 0.02	75.00	1.60 ± 0.05
36.87	1.49 ± 0.02	78.75	1.53 ± 0.05
37.50	1.49 ± 0.03	82.50	1.52 ± 0.05
41.25	1.55 ± 0.02	86.25	1.48 ± 0.06
45.00	1.55 ± 0.02	90.00	1.08 ± 0.04
48.75	1.55 ± 0.02	93.75	1.48 ± 0.05

Our comparision to previous studies is limited to two angles: Schelling *et al.*[3] used a method similar to ours, but with periodic boundary conditions, to simulate (001) Si twist grain boundaries for angles of 11.42°, and 43.60°. Their results indicate Kapitza resistances of 0.61 K m^2/GW, and 1.25 K m^2/GW, respectively, for $T = 500$ K. From theory and further simulations, the thermal boundary resistance is expected to increase for lower temperatures.[18,19] In an estimation, based on results regarding temperature dependency by Aubry *et al.*,[19] we assume that the values of R_K should increase by about 5% to 10%, when the temperature decreases from 500 K to 300 K. Our closest angles for comparison are 11.25°, and 45°. Based on the finite size analysis in Sec. III B, we furthermore reduce our R_K values by 17%, which leads to 0.76 K m^2/GW, and 1.29 K m^2/GW, respectively. Under the preceding considerations, our values agree well with those of Schelling *et al.*,[3] stated above.

Ju and Liang[5] studied (001) Si twist grain boundaries by NEMD simulation with periodic boundary conditions for different temperatures. Their results for $T = 300$ K indicate Kapitza resistances of about 1.5 K m^2/GW, and 2.2 K m^2/GW for angles of 16.26°, and 36.87°, respectively. If we extrapolate our results for these angles from Table III to infinite cross section, our values for R_{inf} reach only about 60% of Ju and Liang's. The deviations might arise due to different methods used during the

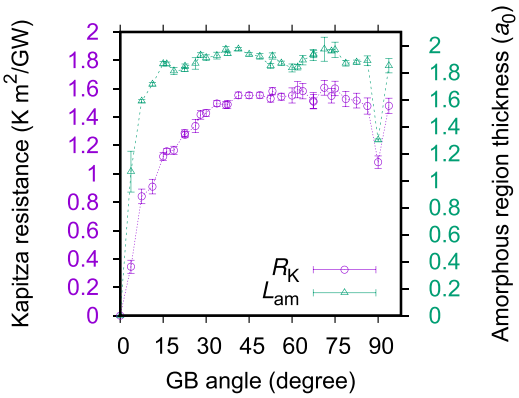

FIG. 11. Dependence of the Kapitza resistance R_K (violett circles, left ordinate) and the thickness of the amorphous region L_{am} in lattice constants (green triangles, right ordinate) on the grain boundary twist angle for a system length of $L = 47.8$ nm and diameter of $D = 6.13$ nm at $T = 300$ K. The measure for the amorphous extent is given by Eq. (5).

equilibration of the grain boundaries prior to the heat flux phase. While we use a *NVT*-thermostat for our fixed boundary conditions, they use a *NPT*-thermostat[11] (with constant pressure P) to relax the system with periodic boundary conditions. Consequently, in our system, we expect both the pressure to be higher and a modified structure of the grain boundary in the vicinity of the fixed walls. However, the differences caused by different configurations should diminish with increasing cross sectional area. Another reason for the deviation of the results might be differences in the heat flux generation, as they use the Müller-Plathe method, while we use velocity rescaling. Nevertheless, the values of R_K are in the same order of magnitude and our simulations yields reasonable information on the grain boundary angle's influence on thermal boundary resistance.

IV. CONCLUSION

We used NEMD to study thermal transport in crystalline ^{28}Si nanowires (length $L \in [24\,\text{nm}, 380\,\text{nm}]$ and diameter $D \in [4\,\text{nm}, 17\,\text{nm}]$) with and without (001) twist grain boundaries. A cylindrical shell of fixed atomistic boundary conditions was used to enable a continuous variation of the twist angle. At first, finite size effects of these boundaries were studied by comparing the heat conductance of the crystalline bulk with other simulations[8] and experimental data.[16] While our NEMD results agree well with simulations of da Cruz *et al.*, compared to experiments the thermal conductivity is overestimated by one order of magnitude, which can be explained by impurities of the crystal lattice in real silicon wires.

Concerning the Kapitza boundary resistance, we noted very little effect due to length variations (see Fig. 8). In contrast, the Kapitza resistance decreased clearly and systematically with the cross sectional area. A linear fit between the inverse Kapitza resistance and the inverse cross section (see Fig. 9) was applied for four different angles to allow an extrapolation to infinite cross section, where the influence of the artificial fixed boundary conditions should vanish. Formally, it also defines a minimal cross section of about 15 unit cells, for which the Kapitza resistance would diverge and which stems from a size independent boundary effect.

The heat conduction was simulated for 33 different (001) twist grain boundaries from 4° to 94° (see Fig. 10) using dimensions of $L \approx 48$ nm and $D \approx 6$ nm. Up to 45°, the Kapitza resistance increased with twist angle. For higher angles, however, up to approx. 80°, the Kapitza resistance reaches a plateau. Finally, it sharply drops by 30% for the 90° $\Sigma 1$ GB system. Except for the latter, no characteristic influence of the CSL grain boundaries compared to adjacent angles could be observed. We explain this by the presence of an amorphous layer: Despite of minute thickness, its disorder renders the effect of the strain relieving coincident sites in the grain boundary irrelevant. Instead, the build-up of this zone of different elasticity during the first 15° constitutes the largest change in R_K. Twisting further, the latter continues to grow, while the thickness stagnates. This suggests a direct influence of the twist angle on the zone's elasticity. The only exception to the CSL-irrelevance is $\vartheta = 90°$, but we can immediately read off Fig. 11 that it is accompanied by a distinct drop of the thickness.

Concerning heat conduction in thermoelectric materials composed of nanoparticles, we conclude that the relative orientation of the grains is of importance, but exhibits less fine structure than expected.

ACKNOWLEDGMENTS

This research has been supported by the German Research Foundation (DFG) (grant no. WO577/10-1 and WO577/6-2) within the priority program SPP 1386 *Nanostructured Thermoelectric Materials: Theory, Model Systems and Controlled Synthesis*.

[1] G. Schierning, J. Stoetzel, R. Chavez, V. Kessler, J. Hall, R. Schmechel, T. Schneider, N. Petermann, H. Wiggers, S. Angst *et al.*, Physica Status Solidi (a) (2016).
[2] S. Uma, A. D. McConnell, M. Asheghi, K. Kurabayashi, and K. E. Goodson, International Journal of Thermophysics **22**, 605 (2001).
[3] P. K. Schelling, S. R. Phillpot, and P. Keblinski, Journal of Applied Physics **95**, 6082 (2004).
[4] T. Watanabe, B. Ni, S. R. Phillpot, P. K. Schelling, and P. Keblinski, Journal of Applied Physics **102**, 063503 (2007).
[5] S. H. Ju and X. G. Liang, Journal of Applied Physics **113**, 053513 (2013).
[6] F. H. Stillinger and T. A. Weber, Physical Review B **31**, 5262 (1985).

[7] S.-C. Wang, X.-G. Liang, X.-H. Xu, and T. Ohara, Journal of Applied Physics **105**, 014316 (2009).
[8] C. A. da Cruz, K. Termentzidis, P. Chantrenne, and X. Kleber, Journal of Applied Physics **110**, 034309 (2011).
[9] S. Plimpton, Journal of Computational Physics **117**, 1 (1995).
[10] F. Müller-Plathe, The Journal of Chemical Physics **106**, 6082 (1997).
[11] S. Nosé, Mol. Phys. **52**, 255 (1984).
[12] P. K. Schelling, S. R. Phillpot, and P. Keblinski, Physical Review B **65**, 144306 (2002).
[13] A. Santoro and A. D. Mighell, Acta Crystallographica Section A **29**, 169 (1973).
[14] J. D. Honeycutt and H. C. Andemen, Journal of Physical Chemistry **91**, 4950 (1987).
[15] D. Li, Y. Wu, P. Kim, L. Shi, P. Yang, and A. Majumdar, Applied Physics Letters **83**, 2934 (2003).
[16] W. S. Capinski, H. J. Maris, E. Bauser, I. Silier, M. Asen-Palmer, T. Ruf, M. Cardona, and E. Gmelin, Applied Physics Letters **71**, 2109 (1997).
[17] A. I. Boukai, Y. Bunimovich, J. Tahir-Kheli, J.-K. Yu, W. A. Goddard, and J. R. Heath, Nature **451**, 168 (2008).
[18] C. Kimmer, S. Aubry, A. Skye, and P. K. Schelling, Physical Review B - Condensed Matter and Materials Physics **75**, 144105 (2007).
[19] S. Aubry, C. J. Kimmer, A. Skye, and P. K. Schelling, Physical Review B - Condensed Matter and Materials Physics **78**, 064112 (2008).